Inorganic Chemistry

Article

pubs.acs.org/IC

Crystal Structure and Magnetic Properties of $FeSeO_3F$—Alternating Antiferromagnetic $S = 5/2$ chains

Shichao Hu,[†] Mats Johnsson,*[,†] Joseph M. Law,[‡] Jerry L. Bettis, Jr.,[§] Myung-Hwan Whangbo,[§] and Reinhard K. Kremer[⊥]

[†]Department of Materials and Environmental Chemistry, Stockholm University, SE-106 91 Stockholm, Sweden

[‡]Dresden High Magnetic Field Laboratory (HLD), Helmholtz-Zentrum Dresden-Rossendorf, D-01328 Dresden, Germany

[§]Department of Chemistry, North Carolina State University, Raleigh, North Carolina 27695-8204, United States

[⊥]Max Planck Institute for Solid State Research, Heisenbergstrasse 1, D-70569 Stuttgart, Germany

Supporting Information

ABSTRACT: The new oxofluoride $FeSeO_3F$, which is isostructural with $FeTeO_3F$ and $GaTeO_3F$, was prepared by hydrothermal synthesis, and its structure was determined by X-ray diffraction. The magnetic properties of $FeSeO_3F$ were characterized by magnetic susceptibility and specific heat measurements, by evaluating its spin exchanges on the basis of density functional theory (DFT) calculations, and by performing a quantum Monte Carlo simulation of the magnetic susceptibility. $FeSeO_3F$ crystallizes in the monoclinic space group $P2_1/n$ and has one unique Se^{4+} ion and one unique Fe^{3+} ion. The building blocks of $FeSeO_3F$ are $[SeO_3]$ trigonal pyramids and *cis*-$[FeO_4F_2]$ distorted octahedra. The *cis*-$[FeO_4F_2]$ octahedra are condensed by sharing the O−O and F−F edges alternatingly to form $[FeO_3F]_\infty$ chains, which are interconnected via the $[SeO_3]$ pyramids by corner-sharing. The magnetic susceptibility of $FeSeO_3F$ is characterized by a broad maximum at 75(2) K and a long-range antiferromagnetic order below ∼45 K. The latter is observed by magnetic susceptibility and specific heat measurements. DFT calculations show that the Fe−F−Fe spin exchange is stronger than the Fe−O−Fe exchange, so each $[FeO_3F]_\infty$ chain is a Heisenberg antiferromagnetic chain with alternating antiferromagnetic spin exchanges. The temperature dependence of the magnetic susceptibility is well-reproduced by a quantum-Monte Carlo simulation.

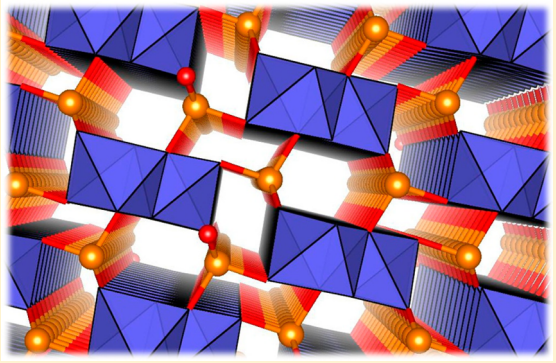

INTRODUCTION

Transition-metal oxides and oxohalides containing a p-block lone pair element have been studied relatively intensively during the past decade. These studies led to several new compounds with interesting physical properties such as magnetic frustration and nonlinear optical second harmonic generation (SHG). Examples include $Cu_2Te_2O_5X_2$,[1] $Ni_5Te_4O_{12}X_2$,[2] $FeTe_2O_5X$,[3] $Ln_3Pb_3O(IO_3)_{13}$ (Ln = La, Pr, Nd),[4] $K(VO)_2O_2(IO_3)_3$,[5] and $Li_6(Mo_2O_5)_3(SeO_3)$.[6] In our synthesis strategy for finding new magnetically interesting compounds, we hypothesize that p-element cations with stereochemically active lone pairs allow for one-sided asymmetric coordination and thus act as "chemical scissors" for opening up crystal structures. In many cases the halide ions Cl^- and Br^- show low coordination number; they can also function as terminating species and reside together with lone-pair elements in nonbonding cavities within the crystal structure due to their suitable ionic radius and weak Lewis base strength.[1−3] In the search for compounds with nonlinear optical SHG, a lone-pair element has been combined with d^0 transition-metal cations possessing second-order Jahn−Teller instability, because this combination increases the chance to find compounds crystallizing in a noncentrosymmetric space group.[4−6] So far, only a limited number of oxofluorides containing lone-pair elements have been reported, which include $V_2Te_2O_7F_2$,[7] $In_3TeO_3F_7$,[8] VBi_2O_5F,[9] $FePbO_2F$,[10] $MTeO_3F$ (M = Fe, Ga),[11] $Co_2TeO_3F_2$, and $Co_2SeO_3F_2$.[12] The difficulty of preparing such compounds originates from the enhanced reactivity of fluoride ions. F^- is smaller in size than Cl^- and Br^- and acts as a bridging ligand between transition-metal cations, as does an O^{2-} ion, rather than as a terminal ligand. This difference is attributed to the smaller radius and stronger electronegativity of fluorine compared to those of chlorine and bromine.

To study the relationship between crystal structures and properties of compounds, it is necessary to prepare phase-pure samples. Most compounds in the M−Q−O−X (M = transition metal; Q = chalcogen, pnictogen; X = halogen) family have been synthesized by solid-state reactions, which usually involve heating, to a high temperature, a sealed evacuated silica ampule containing reagents. It is, however, difficult to obtain M−Q−

Received: February 18, 2014
Published: March 31, 2014

   dx.doi.org/10.1021/ic5003995 | Inorg. Chem. 2014, 53, 4250−4256

O−F compounds using this method because fluorine is so reactive that it corrodes the silica ampule. Even if gold tubes are used, new compounds are often accompanied by impurity phases making it difficult to unravel their magnetic and optical properties. This is the main reason why physical properties have only been studied for a few compounds, for example, $FePbO_2F$.[13] In the present work, we employed the hydrothermal method to synthesize phase-pure samples of $FeSeO_3F$. We characterize the crystal structure of $FeSeO_3F$ by X-ray diffraction, and we characterize its magnetic properties by magnetic susceptibility and specific heat measurements and also by evaluating its spin-exchange interactions on the basis of density functional theory (DFT) calculations and performing quantum Monte Carlo simulations of the magnetic susceptibility.

EXPERIMENTAL SECTION

Single crystals of $FeSeO_3F$ were prepared by hydrothermal synthesis. A mixture of 0.234 g (2.07 mmol) of FeF_3 (Aldrich, 99.9%) and 0.111 g (1.00 mmol) of SeO_2 (Alfa Aesar 99.4%) together with 2 mL of deionized water were sealed in a 23 mL Teflon-lined steel autoclave and heated to 230 °C for 3 d. Yellow block-like single crystals were washed using water and ethanol followed by drying at room temperature. Single-crystal X-ray diffraction data were collected at 293 K on an Oxford Diffraction Xcalibur3 diffractometer using graphite-monochromatized Mo Kα radiation, λ = 0.71073 Å. Absorption correction and data reduction were done with the software CrysAlis RED, which was also employed for the analytical absorption correction.[14] The crystal structure was solved by direct methods using the program SHELXS97 and refined by full matrix least-squares on F^2 using the program SHELXL97.[15] The product purity was confirmed by comparing the experimental X-ray powder diffraction pattern, obtained with a Panalytical X'Pert PRO diffractometer, with a simulated pattern from the crystal structure. All atom positions were refined with anisotropic displacement parameters. Crystal data are reported in Table 1. The coordinates and isotropic temperature parameters for all atoms are given in the Supporting Information. The structural drawings are made with the program DIAMOND.[16] Bond valence sum (BVS) calculations[17,18] give adequate results for all atoms present, see Supporting Information.

The magnetic susceptibilities of a polycrystalline sample (~27.8 mg) were measured in a MPMS SQUID magnetometer (Quantum Design) at various external fields in the temperature range of 1.8 K ≤ T ≤ 300 K. The specific heats were determined using a PPMS system (Quantum Design) in the temperature range of 1.8 K ≤ T ≤ 250 K on a randomly oriented polycrystalline sample of ~2 mg. The specific heats of a minute amount of Apiezon N grease used to thermally couple the sample to the platform and that of the platform were determined in a separate run and subtracted.

RESULTS AND DISCUSSION

Structure Description. The new compound $FeSeO_3F$ crystallizes in the monoclinic space group $P2_1/n$ with unit cell parameters a = 4.9559(5) Å, b = 5.2023(6) Å, c = 12.040(2) Å, and β = 97.87(1)°. The nonstandard setting $P2_1/n$ was used for the refinement rather than $P2_1/c$ due to the more orthogonal β-angle. Experimental parameters are given in Table 1. The crystal structure has one unique Se^{4+} ion and one unique Fe^{3+} ion, and the oxidation states of these ions are supported by BVS calculations.[17,18] The Se atom is bonded to three O at distances in the range of 1.694(6)−1.747(10) Å to form a typical $[SeO_3]$ trigonal pyramid with the stereochemically active lone-electron pair completing a distorted tetrahedron, see Figure 1. Like most other selenites,[19] the $[SeO_3]$ polyhedra of $FeSeO_3F$ do not polymerize. The Fe^{3+} cation has a distorted octahedral coordination *cis*-$[FeO_4F_2]$ with Fe−O bond distances between 1.940(8)−2.090(7) Å and Fe−F bond distances of 1.965(5) and 2.019(7) Å. The *cis*-$[FeO_4F_2]$ octahedra are condensed by alternately sharing the O−O and F−F edges to form $[FeO_3F]_\infty$ zigzag chains extending along [010]. The chains further connect to each other by corner sharing to $[SeO_3]$ trigonal pyramids, see Figure 2. The crystal structure has nonbonding cavities in the form of channels running along [010]. Those channels are formed due to the stereochemically active lone pairs on the $[SeO_3]$ trigonal pyramids.

Table 1. Crystal Data and Structure Refinement Parameters for $FeSeO_3F$

empirical formula	$FeSeO_3F$
formula weight	201.81
temperature (K)	293(2)
wavelength (Å)	0.710 73
crystal system	monoclinic
space group	$P2_1/n$
a (Å)	4.9559(5)
b (Å)	5.2023(6)
c (Å)	12.040(2)
β (deg)	97.87(1)
volume (Å^3)	307.50(6)
Z	4
density$_{calc.}$ (g cm^{-3})	4.359
F(000)	372
crystal color	yellow
crystal habit	block
crystal size (mm)	0.062 × 0.037 × 0.011
theta range for data collection (deg)	3.42 to 28.88
index ranges	$-3 \le h \le 6$
	$-6 \le k \le 6$
	$-15 \le l \le 15$
reflections collected	1744
independent reflections	557[R(int) = 0.0611]
data/restraints/parameters	557/0/55
refinement method	full-matrix least-squares on F^2
goodness-of-fit on F^2	0.817
final R indices [$I > 2\sigma(I)$]^a	R_1 = 0.0278
	wR_2 = 0.0540
R indices (all data)	R_1 = 0.0397
	wR_2 = 0.0559

$^a R_1 = \sum||F_o| - |F_c||/\sum|F_o|$; $wR_2 = \{\sum[w(F_o^2 - F_c^2)^2]/\sum[w(F_o^2)^2]\}^{1/2}$.

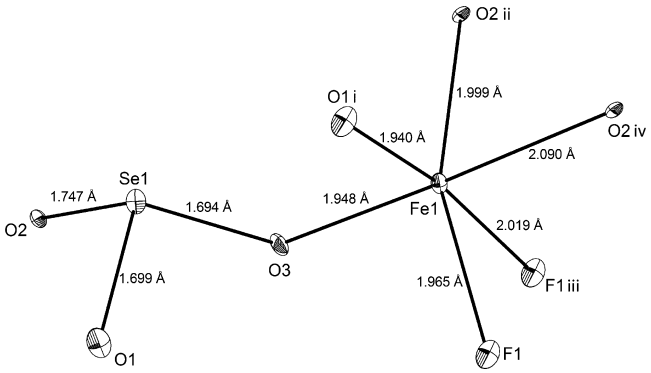

Figure 1. The asymmetric unit and selected equivalents of $FeSeO_3F$. Symmetry codes: (i) 0.5 − x, −0.5 + y, 0.5 − z; (ii) 1.5 − x, −0.5 + y, 0.5 − z; (iii) 1 − x, 1 − y, −z; (iv) −0.5 + x, 0.5 − y, −0.5 + z.

dx.doi.org/10.1021/ic5003995 | Inorg. Chem. 2014, 53, 4250−4256

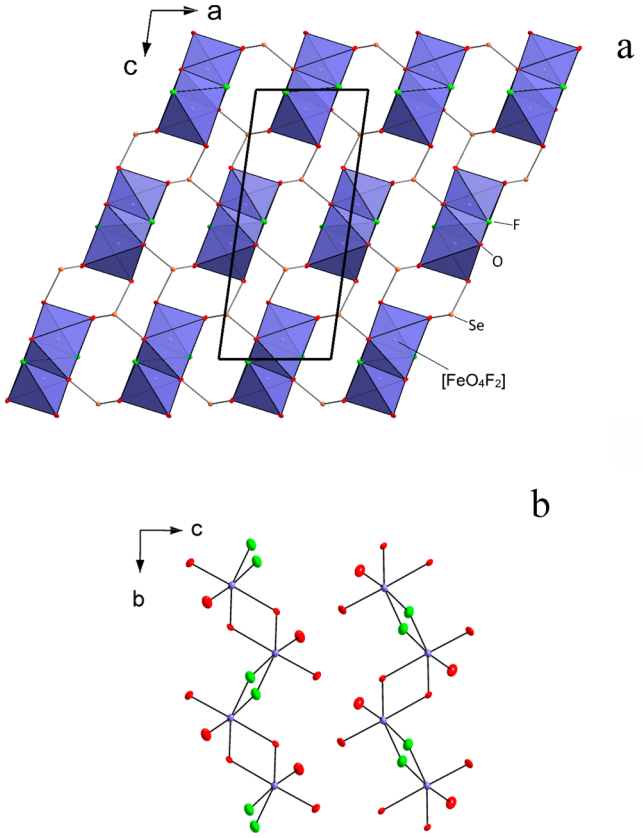

Figure 2. (a) The crystal structure of $FeSeO_3F$ consists of $[FeO_3F]_\infty$ chains made up of edge-sharing *cis*-$[FeO_4F_2]$ octahedra. The chains extend along [010] and are interconnected by $[SeO_3]$ pyramids to form the three-dimensional framework. (b) Schematic view of two $[FeO_3F]_\infty$ zigzag chains along [010], which are made up of *cis*-$[FeO_4F_2]$ octahedra by sharing the O−O and F−F edges alternatingly.

$FeSeO_3F$ is isostructural with the previously described compounds $FeTeO_3F$ and $GaTeO_3F$,[11] which were synthesized by solid-state reactions in gold tubes that did not yield phase-pure products. The unit cell volume of $FeSeO_3F$ is slightly smaller compared to its Te analogue. This difference reflects that the $[SeO_3E]$ tetrahedra are smaller than the $[TeO_3E]$ tetrahedra, where E represents the lone-pair electrons, which in turn reflects that the Se−O bonds are shorter than the Te−O bonds. It has been observed that Se^{4+} and Te^{4+} ions can replace each other when they both take the $[LO_3E]$ (L = Se, Te) coordination, as found for $Co_2TeO_3F_2$ − $Co_2SeO_3F_2$ and $Ni_5(TeO_3)_4Cl_2$ − $Ni_5(SeO_3)_4Cl_2$.[2,12,20] However, many compounds of Te^{4+} ions show either the $[TeO_4E]$ or the $[TeO_5E]$ coordination, which are generally not adopted by Se^{4+} ions. The latter is the main reason why compounds of Te^{4+} ions do not always lead to isostructural Se analogues.

Magnetic and Thermal Properties. The magnetic susceptibility of $FeSeO_3F$ measured in an external field of 0.1 T is displayed in Figure 3a. Measurements at higher fields gave no indication of field dependence. The magnetic susceptibility is characterized by a broad maximum centered at 75(2) K, with a kink at ∼45 K indicating a long-range antiferromagnetic ordering. A plot of the inverse susceptibility versus temperature (Figure 3b) indicates that at sufficiently high temperatures (T > 250 K) the magnetic susceptibility follows a Curie−Weiss law according to

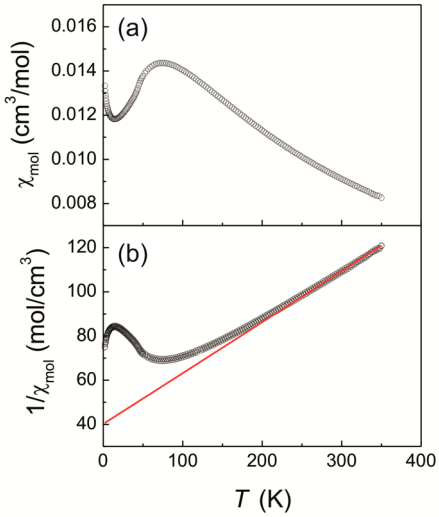

Figure 3. (a) Magnetic susceptibility and (b) inverse magnetic susceptibility of $FeSeO_3F$. The solid straight line represents the Curie−Weiss law with the Curie−Weiss temperature of −175 K.

$$\chi_{spin} = \frac{N_A g^2 2\mu_B^2 S(S+1)}{3k_B(T-\theta)} + \chi_0 \quad (1)$$

where N_A is Avogadro's number, μ_B is the Bohr magneton, k_B is the Boltzmann constant, and χ_0 is the temperature-independent contribution to the susceptibility, which takes account of the diamagnetic contributions of the electrons in closed atom shells and possible van Vleck contributions due to excitations to higher states. Van Vleck contributions in case of a half-filled electronic shell are known to be negligible. The diamagnetic contribution of the closed electronic shell has been estimated to -65×10^{-6} cm^3/mol using Selwood's incremental value for each atom in its respective oxidation state (Fe^{3+}:-0.6×10^{-6} cm^3/mol; Se^{4+}:-11×10^{-6} cm^3/mol; 3 × O^{2-}: -12×10^{-6} cm^3/mol, F^-:-4×10^{-6} cm^3/mol).[21] Fitting the magnetic susceptibility for temperature above 250 K to the Curie−Weiss law (eq 1) converges to a Curie−Weiss temperature of θ = −175(3) K, indicating the presence of predominant antiferromagnetic spin-exchange interactions.

Long-range antiferromagnetic ordering, indicated by a rounded anomaly centered at T_N = 45 K, is found in the specific-heat data displayed in Figure 4b. The magnetic entropy contained in this anomaly amounts to ∼0.7 J/(mol K), which is approximately 5(1)% of the magnetic entropy expected for the ordering of an S = 5/2 spin system [namely, R ln(2S + 1), where R is the molar gas constant and S = 5/2]. The major fraction of the entropy is apparently removed by short-range magnetic ordering spread out over an extended temperature range above T_N. The contribution of the short-range ordering to the heat capacity is difficult to separate from the total heat capacity without a precise knowledge of the lattice phonon contributions.

In Figure 4a we also show the quantity $d(\chi_{mol} \times T)/dT$, sometimes called Fisher's heat capacity.[22] The $d(\chi_{mol} \times T)/dT$ versus T plot also exhibits a peak at 45(1) K, in agreement with the heat capacity data. The low-temperature specific heat deviates somewhat from a power law, $C_p \propto T^3$. This implies that, in addition to the lattice contributions (Debye law), antiferromagnetic magnon contributions are also present.[23]

dx.doi.org/10.1021/ic5003995 | Inorg. Chem. 2014, 53, 4250−4256

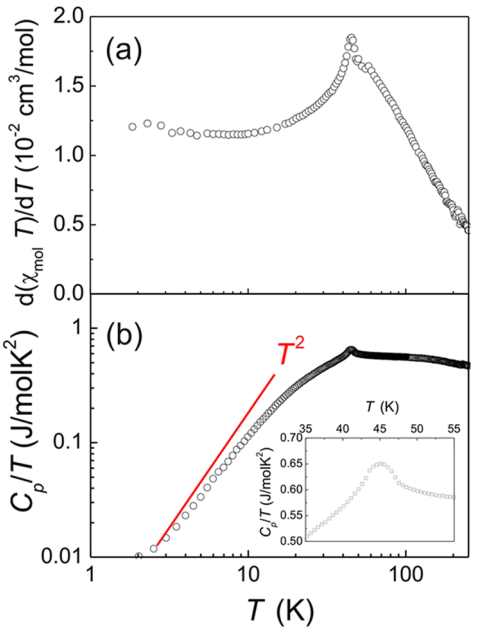

Figure 4. (a) Plot of $d(\chi_{mol}T)/dT$ vs T obtained for $FeSeO_3F$. (b) Specific heat measured for an ensemble of $FeSeO_3F$ crystallites. The solid (red) line represents a T^2 power law. The inset displays the anomaly near 45 K in an enlarged scale.

Theory—Spin Exchange. There are two FeO_3F chains per unit cell, and each FeO_3F chain has alternating Fe−O−Fe and Fe−F−Fe superexchange paths, see Figure 2b. We evaluate the values of these two spin exchanges by performing energy-mapping analysis based on DFT calculations.[24,25] Our DFT electronic structure calculations for $FeSeO_3F$ employed the projected augmented-wave (PAW) method encoded in the Vienna ab initio simulation package[26] and the generalized gradient approximation (GGA) of Perdew, Burke, and Ernzerhof[27] for the exchange-correlation corrections, the plane wave cutoff energy of 400 eV, and the threshold of self-consistent-field (SCF) energy convergence of 10^{-6} eV. The irreducible Brillouin zone was sampled with 64 000 points. To describe the electron correlation associated with the 3d states of Fe, the DFT plus on-site repulsion U (DFT+U)[28] calculations were carried out with effective $U_{eff} = U - J = 4$, 5, and 6 eV on the Fe atoms. To evaluate the Fe−O−Fe and Fe−F−Fe spin exchanges (hereafter, J_1 and J_2, respectively), we consider three ordered spin states FM, AF1, and AF2 presented in Figure 5. The energies of these states can be expressed in terms of the spin Hamiltonian

$$\hat{H} = \sum_{i<j} J_{ij}\hat{S}_i\hat{S}_j \qquad (2)$$

where $J_{ij} = J_1$ and J_2 is the spin-exchange parameter for the interaction between the spin sites i and j. By using the energy expression obtained for spin dimers with N unpaired spins per spin site ($N = 5$),[29] the total spin-exchange energies per formula unit (FU) of the FM, AF1, and AF2 states can be written as

$$E = (c_1J_1 + c_2J_2)(N^2/4) \qquad (3)$$

by applying the energy expressions obtained for spin dimers with N unpaired spins per spin site.[29] The coefficients c_1 and c_2 for the three spin-ordered states are summarized in Figure 5. The relative energies of the FM, AF1, and AF2 states can be calculated on the basis mapping the energy differences between the ordered spin states obtained from the DFT+U calculations onto the corresponding energy differences obtained from the spin Hamiltonian; we obtain the values of J_1 and J_2 summarized in Table 2. The Fe−O−Fe and Fe−F−Fe exchanges are both antiferromagnetic (AFM), and the Fe−F−Fe exchange is slightly stronger than the Fe−O−Fe exchange due probably to the fact that the Fe−F bond is shorter than the Fe−O bond, because the ∠Fe−O−Fe and ∠Fe−F−Fe angles are nearly the same (Supporting Information, Table S2). Each FeO_3F chain forms an alternating AFM chain with a small difference in the two spin exchanges.

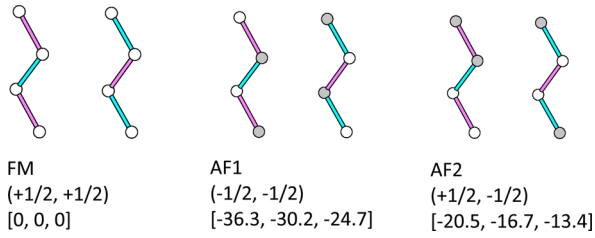

Figure 5. Ordered spin arrangements FM, AF1, and AF2, where the gray and white circles represent the up and down spin sites of Fe^{3+} ions. The cyan and purple cylinders represent the Fe−O−Fe and Fe−F−Fe spin exchange paths J_1 and J_2, respectively. The two numbers (from left to right) in each parentheses represent the coefficients c_1 and c_2 of eq 3, respectively. The three numbers (from left to right) in each square parentheses represent the relative energies obtained from the DFT+U calculations with U_{eff} = 4, 5, and 6 eV, respectively.

Table 2. Spin-Exchange Parameters J_1 and J_2 (in meV) Obtained from the DFT+U Calculations with $U_{eff} = U - J$ = 4, 5, and 6 eV on the Fe Atoms

U_{eff}	4 eV	5 eV	6 eV
J_1	2.5	2.2	1.8
J_2	3.3	2.7	2.1

Quantum Monte Carlo Simulations. As indicated by the DFT calculations the spin exchange between the Fe^{3+} moments must be described essentially by a one-dimensional spin chain with antiferromagnetic spin-exchange interaction. However, because of the alternating superexchange coupling via O^{2-} and F^- anions along the chain (see Figure 1b) spin-exchange constants also alternate between by 10% and 20% along the chain, depending on the choice of the U_{eff}. The magnetic susceptibility of Fe^{3+} ($S = 5/2$) chains have often been approximated by the susceptibility of the Heisenberg chain with classical spins (i.e., $S \rightarrow \infty$).[30] Calculations of the magnetic susceptibility of the classical Heisenberg with alternating spin-exchange interaction have been performed by Duffy and Barr et al.[31] Recently, it has been found that, even for $S = 5/2$ antiferromagnetic Heisenberg chains with uniform nearest-neighbor interaction, quantum effects become important below the characteristic maximum in the susceptibility. Taking into account such corrections provides a noticeable improvement and a better agreement between the experimental and theoretical magnetic susceptibilities, especially at temperatures $T < J$.[32] By directly comparing experimental observables to simulated quantities via density matrix renormalization group (DMRG), quantum Monte Carlo, exact diagonalization etc., one can directly probe the dominant spin-exchanges for various systems.[33]

dx.doi.org/10.1021/ic5003995 | Inorg. Chem. 2014, 53, 4250−4256

To compare our experimental results of the magnetic susceptibility of $FeSeO_3F$ we therefore carried out quantum Monte Carlo calculations of the magnetic susceptibility of an $S = 5/2$ alternating Heisenberg chain described by the Hamiltonian

$$H = \sum_{i}^{N/2} (J_1 \vec{S}_{2i} \vec{S}_{2i-1} + J_2 \vec{S}_{2i} \vec{S}_{2i+1}) \quad (4)$$

where N refers to the total number of spin sites in the alternating chain. We used quantum Monte Carlo via the path integral method of the loop code incorporated within the ALPS project.[34,35] Throughout all simulations a consistent set of steps were used; 15 000 steps were used for thermalization, and 150 000 steps were used after thermalization, ensuring a low statistical error. Additionally, periodic boundary conditions were imposed. So as to reduce finite size effects, the spin susceptibility of the system was calculated for different system sizes at reduced temperatures $T/J_1 = 0.01$. The results are shown in the inset of Figure 6. Size-independent spin

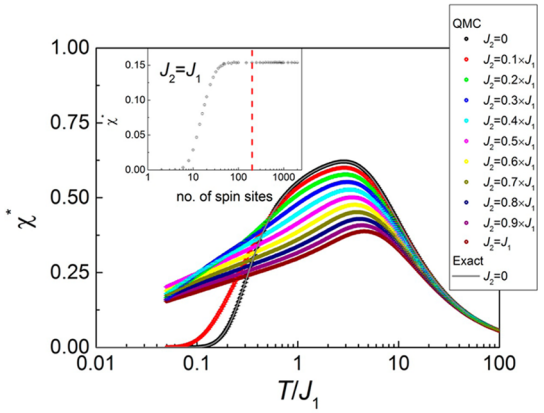

Figure 6. The temperature dependence of the spin susceptibility χ^* (eq 5), simulated by using the quantum Monte Carlo method, for an $S = 5/2$ Heisenberg antiferromagnetic chain with alternating spin exchanges J_1 and J_2. Inset: χ^* for $T/J_1 = 0.01$ calculated for various system sizes. See the text for further details. The dashed (red) line refers to a system size of $N = 200$ spin sites.

susceptibilities are seen for systems of ≥200 spins. Consequently, the choice of the system size was a compromise between the error minimization and the computational-time minimization. Use of the lattice with 500 spin sites yields the percentage error, at the lowest temperature for $J_1 = J_2$, of approximately 0.1%. For convenience we have defined the reduced spin susceptibility (per two $S = 5/2$ entities) according to

$$\chi^* = \chi_{mol}(T, J_1, J_2) \times \frac{2J_1}{N_A \mu_B^2 g^2} \quad (5)$$

The χ^* versus T plots for various ratios of J_2/J_1 are displayed in Figure 6. For comparison with the Monte Carlo results we also plotted the magnetic susceptibility of an $S = 5/2$ dimer (i.e., $J_2 = 0$) calculated using standard techniques from the partition function.[36]

A comparison of the experimental data with the theoretical data is shown in Figure 7. To take account of the slight upturn of the susceptibility at very low temperatures we subtracted a Curie-like susceptibility [$\propto 1/(T + 0.7\ K)$], which we ascribe to

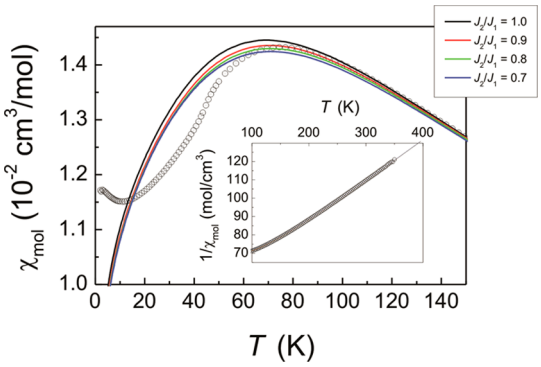

Figure 7. Measured molar magnetic susceptibility corrected for a slight impurity of essentially free spin $S = 5/2$ entities (for details see the text). The (black, red, green, blue) solid lines represent the susceptibilities calculated using eq 6 with the spin-exchange parameters listed in Table 3. The inset displays the inverse susceptibility above 100 K showing a good agreement between the experimental and calculated data.

a small fraction of very weakly coupled $S = 5/2$ spin moments in an amount of 0.001% of the total number of spins. The theoretical curves are plotted for the ratios $J_2/J_1 = 1.0$–0.7. In addition to the susceptibility of the isolated alternating chain, we have also allowed for an interchain coupling, J_{inter}, which leads to the long-range antiferromagnetic ordering at ∼45 K. The interchain coupling was considered by a mean field-type approximation according to

$$\chi_{mol}^{MF} = \frac{\chi_{mol}(J_1, J_2, T)}{1 - \frac{\sum_l z_l J_{l,inter}}{N_A g^2 \mu_{Bohr}^2} \chi_{mol}(J_1, J_2, T)} \quad (6)$$

where $J_{l,inter}$ represents a typical interchain spin-exchange interaction, and N_A is Avogadro's number. A Fe^{3+} ion in a given chain interacts with z_l Fe^{3+} ions in the neighboring chains.

Table 3 lists the exchange parameters used to calculate the theoretical curves in Figure 7. The exchange parameters were

Table 3. Spin-Exchange Parameter Used to Calculate the Solid Lines in Figure 6 Using eq 6. The Rightmost Column Gives the Curie-Weiss Temperature Calculated According to eq 7

J_2/J_1	J_1 (K)	$-\sum_l z_l J_{l,inter}$(K)	$\theta = \theta_{intra} + \theta_{inter}$ (K)
1.0	15.15	−25.4	−163
0.9	16.25	−24.5	−162
0.8	17.25	−24.2	−161
0.7	18.25	−24.3	−161

chosen such that the calculated data match the high-temperature Curie–Weiss susceptibility well and also approach the broader maximum at low temperatures. Since we have no information on how moments in the neighboring chains interact with a central chain we have instead given the quantity $\sum_l z_l J_{l,inter}$ in Table 3. If we assume an average $z_l \approx 4$–6, the characteristic interchain spin-exchange interaction amounts to $\overline{J}_{inter} \approx -6$ to -4 K, accounting for the long-range antiferromagnetic ordering at ∼45 K. A high-temperature expansion of eq 6 leads to a Curie–Weiss law expressed as

$$\chi_{mol}^{HT} = \frac{C}{T - (\theta_{intra} + \theta_{inter})} \quad (7)$$

dx.doi.org/10.1021/ic5003995 | Inorg. Chem. 2014, 53, 4250–4256

where the Curie–Weiss temperatures θ_{intra} and θ_{inter} are given by

$$\theta_{intra} = -\frac{1}{3}S(S+1)(J_1 + J_2) \quad (8a)$$

$$\theta_{inter} = -\frac{1}{3}S(S+1)\sum_j z_j J'_j \quad (8b)$$

where J'_j refers to the interchain spin exchanges that were not evaluated in the present work. Using eqs 7 and 8 we have calculated the Curie–Weiss temperatures listed in the rightmost column of Table 3. They are approximately −162 K, which is consistent with the result of the Curie–Weiss fit discussed above.

CONCLUDING REMARKS

By hydrothermal synthesis, we prepared single crystals of $FeSeO_3F$, which crystallizes in the monoclinic space group $P2_1/n$ with the unit cell parameters a = 4.9559(5) Å, b = 5.2023(6) Å, c = 12.040(2) Å, β = 97.87(1)°, and Z = 4. $FeSeO_3F$ has one unique Se^{4+} ion and one unique Fe^{3+} ion, with building blocks of $[SeO_3]$ trigonal pyramids and *cis*-$[FeO_4F_2]$ distorted octahedra. The *cis*-$[FeO_4F_2]$ octahedra are condensed by sharing the O–O and F–F edges alternatingly to form $[FeO_3F]_\infty$ chains, which are separated by corner sharing $[SeO_3]$ units. $FeSeO_3F$ is isostructural with the previously described compounds $FeTeO_3F$ and $GaTeO_3F$.

The magnetic susceptibility of $FeSeO_3F$ is well-described by a chain of alternating antiferromagnetic intrachain spin-exchanges. Weak interchain interactions lead to the long-range antiferromagnetic ordering below ∼45 K, evidenced by magnetic susceptibility and specific heat measurements. Our magnetic susceptibility data were analyzed by evaluating the intrachain Fe–F–Fe and Fe–O–Fe spin exchanges on the basis of DFT calculations and by performing a quantum Monte Carlo simulation of the magnetic susceptibility of an antiferromagnetic S = 5/2 linear chain with alternating antiferromagnetic spin exchanges.

ASSOCIATED CONTENT

Supporting Information

Tables of atomic coordinates and equivalent isotropic displacement parameters, bonding distances and angles, and BVS calculations. This material is available free of charge via the Internet at http://pubs.acs.org. Further details on the crystal structural investigations can be obtained from the Fachinformationszentrum Karlsruhe, Abt. PROKA, 76344 Eggenstein-Leopoldshafen, Germany (fax +49–7247–808–666; E-mail: crysdata@fiz-karlsruhe.de) on quoting the depository number CSD-427332.

AUTHOR INFORMATION

Corresponding Author

*Email: mats.johnsson@mmk.su.se. Phone: +46-8-162169. Fax: +46-8-152187.

Notes

The authors declare no competing financial interest.

ACKNOWLEDGMENTS

This work was in part carried out through financial support from the Swedish Research Council. We thank Mrs. E. Brücher and Mrs. G. Siegle for expert experimental assistance and also the support of the HLD at HZDR, member of the European Magnetic Field Laboratory (EMFL). Work at NCSU was supported by the computing resources of the NERSC Center and the HPC Center of NCSU.

REFERENCES

(1) Johnsson, M.; Törnroos, K. W.; Mila, F.; Millet, P. *Chem. Mater.* **2000**, *12*, 2853–2857.
(2) Johnsson, M.; Törnroos, K. W.; Lemmens, P.; Millet, P. *Chem. Mater.* **2003**, *15*, 68–73.
(3) Becker, R.; Johnsson, M.; Kremer, R. K.; Klauss, H.-H.; Lemmens, P. *J. Am. Chem. Soc.* **2006**, *128*, 15469–15475.
(4) Hu, T.; Qin, L.; Kong, F.; Zhou, Y.; Mao, J.-G. *Inorg. Chem.* **2009**, *48*, 2193–2199.
(5) Sun, C.-F.; Hu, C.-L.; Xu, X.; Yang, B.-P.; Mao, J.-G. *J. Am. Chem. Soc.* **2011**, *133*, 5561–5572.
(6) Nguyen, S. D.; Halesyamani, P. S. *Inorg. Chem.* **2012**, *51*, 9529–9538.
(7) Laval, J. P.; Boukharrata, N. J. *Acta Crystallogr.* **2009**, *C65*, i1.
(8) Boukharrata, N. J.; Laval, J. P. *J. Alloys Compd.* **2011**, *509*, 1517–1522.
(9) Akopjan, A. V.; Serov, T. V.; Dolgikh, V. A.; Ardashnikova, E. I.; Lightfoot, P. *J. Mater. Chem.* **2002**, *12*, 1490–1494.
(10) Inaguma, Y.; Greneche, J. M.; Crosnier-Lopez, M. P.; Katsumata, T.; Calage, Y.; Fourquet, J. L. *Chem. Mater.* **2005**, *17*, 1386–1390.
(11) Laval, J. P.; Boukharrata, N. J.; Thomas, P. *Acta Crystallogr.* **2008**, *C64*, i12.
(12) Hu, S.; Johnsson, M . *Dalton Trans.* **2012**, *41*, 12786–12789.
(13) Katsumata, T.; Nakashima, M.; Umemoto, H.; Inaguma, Y. *J. Solid State Chem.* **2008**, *181*, 2737–2740.
(14) *Oxford Diffraction (2006), CrysAlis CCD, and CrysAlis RED;* Oxford Diffraction Ltd.: Abingdon, Oxfordshire, England.
(15) Sheldrick, G. M. *Acta Crystallogr., Sect. A* **2008**, *A64*, 112–122.
(16) Bergerhoff, G. *DIAMOND;* University of Bonn: Bonn, Germany, 1996.
(17) Brown, I. D.; Altermatt, D. *Acta Crystallogr.* **1985**, *B41*, 244–247.
(18) Brese, N. E.; O'Keeffe, M. *Acta Crystallogr.* **1991**, *B47*, 192–197.
(19) Mao, J.-G.; Jiang, H.-L.; Kong, F. *Inorg. Chem.* **2008**, *47*, 8498–8510.
(20) Shen, Y.; Mao, J.; Jiang, H. *J. Solid State Chem.* **2005**, *178*, 2942–2946.
(21) Selwood, P. W. *Magnetochemistry;* Interscience: New York, 1943.
(22) Fisher, M. E. *Philos. Mag.* **1962**, *7*, 1731–1743.
(23) de Jongh, L. J.; Miedema, A. R. *Adv. Phys.* **1974**, *23*, 1–260.
(24) Whangbo, M.-H.; Koo, H.-J.; Dai, D. *J. Solid State Chem.* **2003**, *176*, 417–481 and the references cited therein.
(25) Xiang, H. J.; Lee, C.; Koo, H.-J.; Gong, X. G.; Whangbo, M.-H. *Dalton Trans.* **2013**, *42*, 823–853 and the references cited thererin.
(26) (a) Kresse, G.; Hafner, J. *Phys. Rev. B* **1993**, *62*, 558–561. (b) Kresse, G.; Furthmüller, J. *Comput. Mater. Sci.* **1996**, *6*, 15–50. (c) Kresse, G.; Furthmüller, J. *Phys. Rev. B* **1996**, *54*, 11169–11186.
(27) Perdew, J. P.; Burke, S.; Ernzerhof, M. *Phys. Rev. Lett.* **1996**, *77*, 3865–3868.
(28) Dudarev, S. L.; Botton, G. A.; Savrasov, S. Y.; Humphreys, C. J.; Sutton, A. P. *Phys. Rev. B* **1998**, *57*, 1505–1509.
(29) (a) Dai, D.; Whangbo, M.-H. *J. Chem. Phys.* **2001**, *114*, 2887–2893. (b) Dai, D.; Whangbo, M.-H. *J. Chem. Phys.* **2003**, *118*, 29–39.
(30) Fisher, M. E. *J. Math. Phys.* **1963**, *4*, 124–135.
(31) Duffy, W., jr.; Barr, K. P. *Phys. Rev.* **1968**, *165*, 647–654.
(32) Law, J. M.; Benner, H.; Kremer, R. K. *J. Phys.: Condens. Matter.* **2013**, *25*, 065601.
(33) (a) Kampert, E.; Janssen, F. F. B. J.; Boukhvalov, D. W.; Russcher, J. C.; Smits, J. M. M.; de Gelder, R.; de Bruin, B.; Christianen, P. C. M.; Zeitler, U.; Katsnelson, M. I.; Maan, J. C.; Rowan, A. E. *Inorg. Chem.* **2009**, *48*, 11903–11908. (b) Law, J. M;

Hoch, C.; Whangbo, M-H; Kremer, R. K. *Z. Anorg. Allg. Chem.* **2010**, *636*, 54−61. (c) Law, J. M.; Hoch, C.; Glaum, R.; Heinmaa, I.; Stern, R.; Whangbo, M-H; Kremer, R. K. *Phys. Rev. B.* **2011**, *83*, 180414. (d) Law, J. M.; Reuvekamp, P.; Glaum, R.; Lee, C.; Kang, J.; Whangbo, M.-H.; Kremer, R. K. *Phys. Rev. B.* **2011**, *84*, 014426. (e) Janson, O.; Tsirlin, A. A.; Sichelschmidt, J.; Skourski, Yu.; Weickert, F.; Rosner, H. *Phys. Rev. B.* **2011**, *83*, 094435. (f) Bera, A. K.; Lake, B.; Islam, A. T. M. N.; Klemke, B.; Faulhaber, E.; Law, J. M. *Phys. Rev. B.* **2013**, *87*, 224423/1−10. (g) Caslin, K.; Kremer, R. K.; Razavi, F. S.; Schulz, A.; Muñoz, A.; Pertlik, F.; Liu, J.; Whangbo, M.-H.; Law, J. M. *Phys. Rev. B.* **2014**, *89*, 014412. (h) Law, J. M.; Koo, H.-J.; Whangbo, M.-H.; Bruecher, E.; Pomjakushin, V.; Kremer, R. K. *Phys. Rev. B.* **2014**, *89*, 014423.

(34) Albuquerque, A. F.; Alet, F.; Corboz, P.; Dayal, P.; Feiguin, A.; Fuchs, S.; Gamper, L.; Gull, E.; Gürtler, S.; Honecker, A.; Igarashi, R.; Körner, M.; Kozhevnikov, A.; Läuchli, A.; Manmana, S. R.; Matsumoto, M.; McCulloch, I. P.; Michel, F.; Noack, R. M.; Pawlowski, G.; Pollet, L.; Pruschke, T.; Schollwöck, U.; Todo, S.; Trebst, S.; Troyer, M.; Werner, P.; Wessel, S. *J. Magn. Magn. Mater.* **2007**, *310*, 1187−1193[89.

(35) Todo, S.; Kato, K. *Phys. Rev. Lett.* **2001**, *87*, 047203.

(36) Lueken, H. *Magnetochemie;* Stuttgart: Teubner Studienbücher, 1999.